


Study of the $\chi_{cJ} \rightarrow \Lambda\bar{\Lambda}\eta'$ decays

M. Ablikim *et al.**
(BESIII Collaboration)

 (Received 26 August 2025; accepted 28 October 2025; published 18 December 2025)

Using a data sample of $(2.712 \pm 0.014) \times 10^9$ $\psi(3686)$ events collected with the BESIII detector at the BEPCII collider, we investigate the decays $\chi_{cJ} \rightarrow \Lambda\bar{\Lambda}\eta'$ for $J = 0, 1, 2$ via the radiative transition $\psi(3686) \rightarrow \gamma\chi_{cJ}$. The decays $\chi_{c0,2} \rightarrow \Lambda\bar{\Lambda}\eta'$ are observed for the first time, with statistical significances of 6.7σ and 6.4σ , respectively. Evidence for the decay $\chi_{c1} \rightarrow \Lambda\bar{\Lambda}\eta'$ is found with a statistical significance of 3.3σ . The corresponding branching fractions are measured to be $\mathcal{B}(\chi_{c0} \rightarrow \Lambda\bar{\Lambda}\eta') = (7.56 \pm 1.42 \pm 0.90) \times 10^{-5}$, $\mathcal{B}(\chi_{c1} \rightarrow \Lambda\bar{\Lambda}\eta') = (1.54 \pm 0.51 \pm 0.16) \times 10^{-5}$, and $\mathcal{B}(\chi_{c2} \rightarrow \Lambda\bar{\Lambda}\eta') = (3.03 \pm 0.61 \pm 0.29) \times 10^{-5}$, where the first uncertainties are statistical and the second are systematic. No significant excited Λ baryon states or $\Lambda\bar{\Lambda}$ near-threshold enhancements are observed.

DOI: [10.1103/9kcj-rp8r](https://doi.org/10.1103/9kcj-rp8r)

I. INTRODUCTION

The χ_{cJ} ($J = 0, 1, 2$) mesons are the P -wave spin-triplet charmonium states in the quark model. Compared with the extensively studied decays of the S -wave charmonia J/ψ and $\psi(3686)$, the decays of χ_{cJ} remain less thoroughly investigated both experimentally and theoretically. Their direct production in e^+e^- annihilation is strongly suppressed since they involve processes with two virtual photons or neutral currents; to date, only the χ_{c1} state has been observed at BESIII with a significance of 5.1σ [1] in these processes. An efficient production mechanism for the χ_{cJ} states is provided by the radiative transitions $\psi(3686) \rightarrow \gamma\chi_{cJ}$, whose branching fractions are approximately 10% for each χ_{cJ} state. This enables precision studies of χ_{cJ} decays with a large $\psi(3686)$ data sample.

Decays of χ_{cJ} mesons into baryon-antibaryon-meson ($B\bar{B}M$) final states offer a unique opportunity to investigate $B\bar{B}$ threshold behaviour and excited baryon states in the BM system, where B and \bar{B} denote a baryon and its antibaryon, respectively, and M represents a meson. Recently, evidence for a resonance Λ^* was reported in the invariant-mass spectrum of $\Lambda(\bar{\Lambda})$ and ω in the decay $\psi(3686) \rightarrow \Lambda\bar{\Lambda}\omega$ [2]. Although $\Lambda\bar{\Lambda}$ mass-threshold enhancements have been observed in $e^+e^- \rightarrow \Lambda\bar{\Lambda}\phi$ [3] and $e^+e^- \rightarrow \Lambda\bar{\Lambda}\eta$ [4], significant discrepancies in the magnitude of the enhancements are evident between the two channels. The $\chi_{cJ} \rightarrow B\bar{B}M$

decay channels ($\chi_{cJ} \rightarrow \Lambda\bar{\Lambda}\eta$ [5], $\Lambda\bar{\Lambda}\omega$ [6], $\Lambda\bar{\Lambda}\phi$ [7], and $\Sigma^+\bar{\Sigma}^-\eta$ [8]) have been exploited to search for such enhancements, but no conclusive evidence has yet been obtained.

In this paper, we investigate the decays $\chi_{cJ} \rightarrow \Lambda\bar{\Lambda}\eta'$ using a data sample of $(2.712 \pm 0.014) \times 10^9$ $\psi(3686)$ events [9] collected with the BESIII detector. The Λ and $\bar{\Lambda}$ baryons are reconstructed via $\Lambda \rightarrow p\pi^-$ and $\bar{\Lambda} \rightarrow \bar{p}\pi^+$, respectively. The η' meson is reconstructed through two decay modes: $\eta' \rightarrow \gamma\pi^+\pi^-$ (mode I) and $\eta' \rightarrow \eta\pi^+\pi^-$ with $\eta \rightarrow \gamma\gamma$ (mode II). The branching fractions of $\chi_{cJ} \rightarrow \Lambda\bar{\Lambda}\eta'$ are measured for the first time. In addition, possible Λ^* excited states and near-threshold enhancement in the $\Lambda\bar{\Lambda}$ system are investigated.

II. BESIII DETECTOR AND MONTE CARLO SIMULATION

The BESIII detector [10] records symmetric e^+e^- collisions provided by the BEPCII storage ring [11] in the center-of-mass energy range from 1.84 to 4.95 GeV, with a peak luminosity of $1.1 \times 10^{33} \text{ cm}^{-2} \text{ s}^{-1}$ achieved at $\sqrt{s} = 3.773$ GeV. BESIII has collected large data samples in this energy region [12–14]. The cylindrical core of the BESIII detector covers 93% of the full solid angle and consists of a helium-based multilayer drift chamber (MDC), a time-of-flight system (TOF), and a CsI(Tl) electromagnetic calorimeter (EMC), which are all enclosed in a superconducting solenoidal magnet providing a 1.0 T magnetic field. The solenoid is supported by an octagonal flux-return yoke with resistive plate counter muon identification modules interleaved with steel. The charged-particle momentum resolution at 1 GeV/ c is 0.5%, and the dE/dx resolution is 6% for electrons from Bhabha scattering. The EMC measures photon energies with a resolution of 2.5% (5%) at 1 GeV in the barrel (end cap) region. The time resolution in

*Full author list given at the end of the article.

Published by the American Physical Society under the terms of the [Creative Commons Attribution 4.0 International license](https://creativecommons.org/licenses/by/4.0/). Further distribution of this work must maintain attribution to the author(s) and the published article's title, journal citation, and DOI. Funded by SCOAP³.

the plastic scintillator TOF barrel region is 68 ps, while that in the end cap region was 110 ps. The end cap TOF system was upgraded in 2015 using multigap resistive plate chamber technology, providing a time resolution of 60 ps, which benefits 83% of the data used in this analysis [15].

Monte Carlo (MC) simulated data samples produced with a GEANT4-based [16] software package, which includes the geometric description of the BESIII detector and the detector response, are used to determine detection efficiencies and to estimate backgrounds. The simulation models the beam energy spread and initial state radiation (ISR) in the e^+e^- annihilations with the generator KKMC [17]. The inclusive MC sample includes the production of the $\psi(3686)$ resonance, the ISR production of the J/ψ , and the continuum processes incorporated in KKMC [17]. All particle decays are modeled with EVTGEN [18] using branching fractions either taken from the Particle Data Group (PDG) [19], when available, or otherwise estimated with LUNDCHARM [20]. Final-state radiation from charged final-state particles is incorporated using the PHOTOS package [21].

The signal MC events of the $\psi(3686) \rightarrow \gamma\chi_{cJ}$ decays follow the angular distribution of $1 + \lambda \cos^2 \theta_\gamma$, where θ_γ denotes the polar angle of the radiative photon, and λ takes the values 1, $-1/3$, and $1/13$ for $J = 0, 1$, and 2 , respectively [22]. For subsequent decays, the processes $\chi_{cJ} \rightarrow \Lambda\bar{\Lambda}\eta'$ are modeled using a phase-space (PHSP) model. The decay $\eta' \rightarrow \gamma\pi^+\pi^-$ is implemented via a model [23] that incorporates the $\rho - \omega$ interference effects and the box anomaly mechanism. The decay $\eta' \rightarrow \eta\pi^+\pi^-$ is generated according to the Dalitz distribution of the Ref. [24] with the subsequent decay of $\eta \rightarrow \gamma\gamma$ following a PHSP model. The processes of $\Lambda \rightarrow p\pi^-$ and $\bar{\Lambda} \rightarrow \bar{p}\pi^+$ are generated by the HypWK model [18], which is constructed for spin- $\frac{1}{2}$ hyperon and its antihyperon nonleptonic decays including parity-violation effects.

III. EVENT SELECTION

Candidate events are required to have the final states $p\bar{p}\pi^+\pi^-\pi^+\pi^-2\gamma$ (mode I) and $p\bar{p}\pi^+\pi^-\pi^+\pi^-3\gamma$ (mode II). Charged tracks detected in the MDC are required to be within a polar angle range of ($|\cos\theta| < 0.93$), where θ is defined with respect to the z axis, which is the symmetry axis of the MDC. At least three positive and three negative tracks are required for each mode. Λ and $\bar{\Lambda}$ candidates are reconstructed by pairing oppositely charged tracks with proton and pion mass hypotheses, respectively. Each pair is subjected to a primary vertex fit followed by a secondary vertex fit; the latter is applied to reconstruct long-lived resonances [25]. The optimal combination is selected by minimizing the mass deviation, defined as $\Delta = \sqrt{(M(p\pi^-) - m_\Lambda)^2 + (M(\bar{p}\pi^+) - m_{\bar{\Lambda}})^2}$, where $M(p\pi^-)$ and $M(\bar{p}\pi^+)$ are the invariant masses of $p\pi^-$ and $\bar{p}\pi^+$, respectively, and $m_{\Lambda(\bar{\Lambda})}$ denotes the $\Lambda(\bar{\Lambda})$

nominal mass [19]. Tracks not associated with Λ or $\bar{\Lambda}$ are required to originate from the interaction point (IP) within 10 cm along the z axis and 1 cm in the transverse plane. Exactly two such tracks with zero net charge are retained and assigned the pion mass hypothesis; they are subjected to a vertex fit to confirm their common origin.

Photon candidates are identified from showers in the EMC. The deposited energy of each shower must be more than 25 MeV in the barrel region ($|\cos\theta| < 0.80$) and more than 50 MeV in the end cap region ($0.86 < |\cos\theta| < 0.92$). To exclude showers that originate from charged tracks, the angle subtended by the EMC shower and the position of the closest charged track at the EMC must be greater than 10 deg as measured from the IP. To suppress electronic noise and showers unrelated to the event, the difference between the EMC time and the event start time must be within [0, 700] ns. At least two (three) photons are required for mode I (mode II).

To improve mass resolution and suppress background, a four-constraint (4C) kinematic fit is applied to mode I, constraining the total 4-momentum of the final-state particles to that of the colliding beams. When more than two photon candidates are present, the combination with the least χ_{4C}^2 is selected, satisfying $\chi_{4C}^2 < 18$. The photon originating from the η' decay is identified as the one that minimizes $|M(\gamma\pi^+\pi^-) - m_{\eta'}|$, where $M(\gamma\pi^+\pi^-)$ is the reconstructed invariant mass of $\gamma\pi^+\pi^-$, and $m_{\eta'}$ is the η' nominal mass [19]. For mode II, a five-constraint (5C) kinematic fit is implemented: a 4C kinematic fit together with an additional constraint on the two photons from the η candidate to the η nominal mass [19]. When more than three photon candidates are present, the combination with the least χ_{5C}^2 is chosen, requiring $\chi_{5C}^2 < 53$. The χ^2 requirements for both modes are optimized by maximizing the figure of merit $S/\sqrt{S+B}$, where $S(B)$ is the number of signal (background) events from the normalized signal (inclusive) MC sample. In addition, the criterion $\chi_{4C,n\gamma}^2 < \chi_{4C,(n+1)\gamma}^2$ is applied for both modes, where n is the expected number of photons in the signal process. The $\Lambda(\bar{\Lambda})$ signal region is defined as $|M(p\pi^-) - m_\Lambda| < 5 \text{ MeV}/c^2$ ($|M(\bar{p}\pi^+) - m_{\bar{\Lambda}}| < 5 \text{ MeV}/c^2$). The decay length of $\Lambda(\bar{\Lambda})$ candidate, defined as the distance between its production and decay point, is required to be larger than 0, with a resolution of the detector of 0.6 cm. The expected decay length of $\Lambda(\bar{\Lambda})$ is 7.9 cm [19]. Figure 1 shows the distributions of $M(\bar{p}\pi^+)$ versus $M(p\pi^-)$ for mode I and mode II for the surviving candidates in the data. The box outlined by red solid lines is the two-dimensional (2D) $\Lambda\bar{\Lambda}$ signal region, and the boxes outlined by pink and blue dashed lines are 2D $\Lambda\bar{\Lambda}$ sideband regions. A clear $\Lambda\bar{\Lambda}$ pair signal is found in the distribution. The events in the 2D $\Lambda\bar{\Lambda}$ sideband regions are used to estimate the non- $\Lambda\bar{\Lambda}$ background in the 2D $\Lambda\bar{\Lambda}$ signal region.

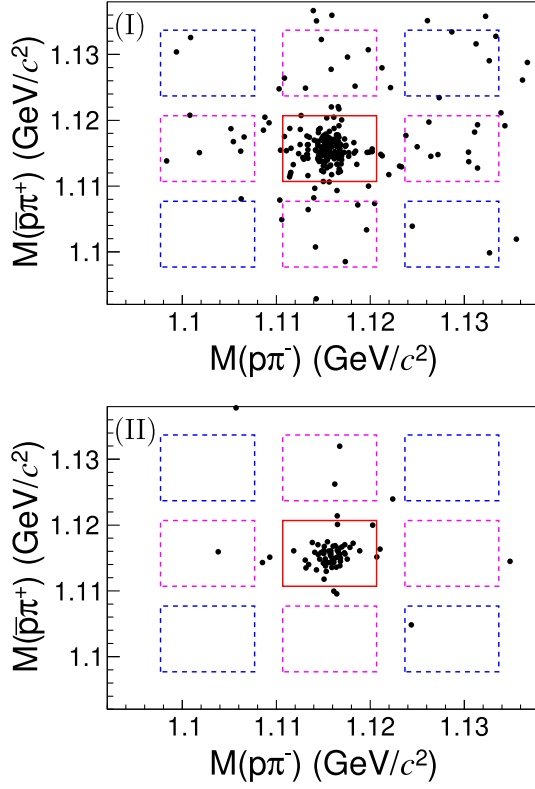


FIG. 1. The scatter plots of $M(\bar{p}\pi^+)$ versus $M(p\pi^-)$ for mode I and mode II from the survived candidates in data, where the red solid box is the 2D $\Lambda\bar{\Lambda}$ signal region and the pink and blue dashed boxes are the 2D $\Lambda\bar{\Lambda}$ sideband regions.

For mode I, the directly emitted photon is labeled γ_1 , and that from the η' decay is labeled γ_2 . After applying the aforementioned selection criteria, three types of background processes remain: the $\Sigma^0(\bar{\Sigma}^0)$ -related backgrounds, the J/ψ -related backgrounds, and the π^0 -related backgrounds. To suppress the $\Sigma^0(\bar{\Sigma}^0)$ -related backgrounds, we require the invariant mass of the $\Lambda/\bar{\Lambda}$ combined with either photon candidate to satisfy $M(\Lambda(\bar{\Lambda})\gamma_{1,2}) > 1.2 \text{ GeV}/c^2$. The J/ψ -related backgrounds are mitigated by excluding events where the recoil mass of the $\pi^+\pi^-$ system and $\gamma_1\gamma_2$ system fall within the J/ψ mass window, $|RM(\pi^+\pi^-) - m_{J/\psi}| > 10 \text{ MeV}/c^2$ and $|RM(\gamma_1\gamma_2) - m_{J/\psi}| > 26 \text{ MeV}/c^2$, where the $\pi^+\pi^-$ from the η' decay. The π^0 -related backgrounds are suppressed by vetoing the π^0 mass region in the $\gamma_1\gamma_2$ invariant mass distribution, $|M(\gamma_1\gamma_2) - m_{\pi^0}| > 14 \text{ MeV}/c^2$. The η' signal region is set to be $[m_{\eta'} - 12, m_{\eta'} + 12] \text{ MeV}/c^2$, with η' sideband regions $[m_{\eta'} - 60, m_{\eta'} - 36] \cup [m_{\eta'} + 36, m_{\eta'} + 60] \text{ MeV}/c^2$ used to estimate the non- η' background in the η' signal region. For mode II, the requirement of $M(\Lambda(\bar{\Lambda})\gamma) > 1.2 \text{ GeV}/c^2$ is used to reject the $\Sigma^0(\bar{\Sigma}^0)$ -related backgrounds. The η' signal region is tightened to $[m_{\eta'} - 10, m_{\eta'} + 10] \text{ MeV}/c^2$, with the η' sideband regions set to

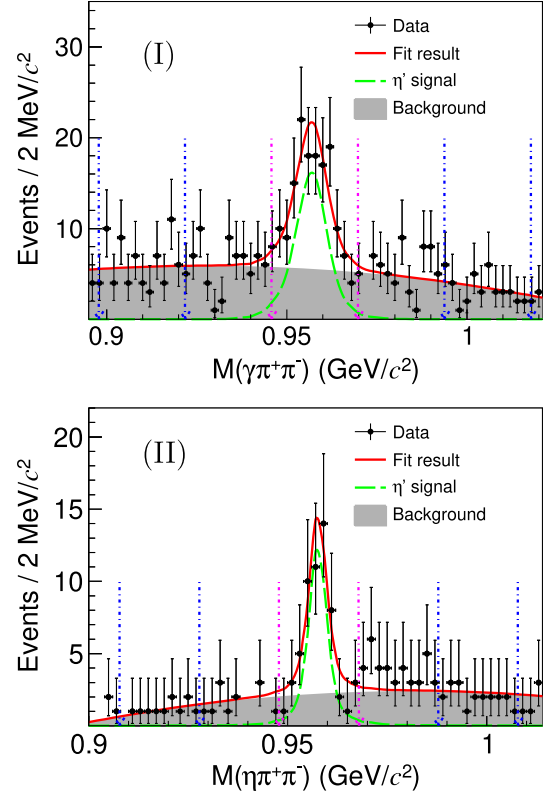


FIG. 2. The distributions of $M(\gamma\pi^+\pi^-)$ for mode I and $M(\eta\pi^+\pi^-)$ for mode II. The pink arrows mark the η' signal region, and the two pairs of blue arrows mark the η' sideband regions. The dots with error bars are data, the red solid lines are the fit results, the green dashed lines represent the signal shapes, and the gray shaded histograms constitute the smooth backgrounds.

be $[m_{\eta'} - 50, m_{\eta'} - 30] \cup [m_{\eta'} + 30, m_{\eta'} + 50] \text{ MeV}/c^2$. Figure 2 shows the distributions of $M(\gamma\pi^+\pi^-)$ for mode I and $M(\eta\pi^+\pi^-)$ for mode II in data, with the η' signal and sideband regions indicated.

IV. BRANCHING FRACTIONS

The branching fractions of $\chi_{cJ} \rightarrow \Lambda\bar{\Lambda}\eta'$ are determined using a simultaneous unbinned maximum-likelihood fit to the distributions of the invariant masses of $M(\Lambda\bar{\Lambda}\gamma\pi^+\pi^-)$ for mode I and $M(\Lambda\bar{\Lambda}\eta\pi^+\pi^-)$ for mode II. The fit is performed in both the η' signal and sideband regions. In the simultaneous fit, a common branching fraction $\mathcal{B}(\chi_{cJ} \rightarrow \Lambda\bar{\Lambda}\eta')$ is shared between the two modes. Furthermore, the parameters describing the shape of the non- η' background in the η' signal region are determined from and shared with the shape of the events in the η' sideband regions. For mode I, the events in the η' sideband regions are used to estimate the non- η' background in the η' signal region. The non- $\Lambda\bar{\Lambda}$ background is found to be negligible using the events in the 2D $\Lambda\bar{\Lambda}$ sideband regions in Fig. 1. Figures 3(a) and 3(b) show the distributions of $M(\Lambda\bar{\Lambda}\gamma\pi^+\pi^-)$ in the η' signal

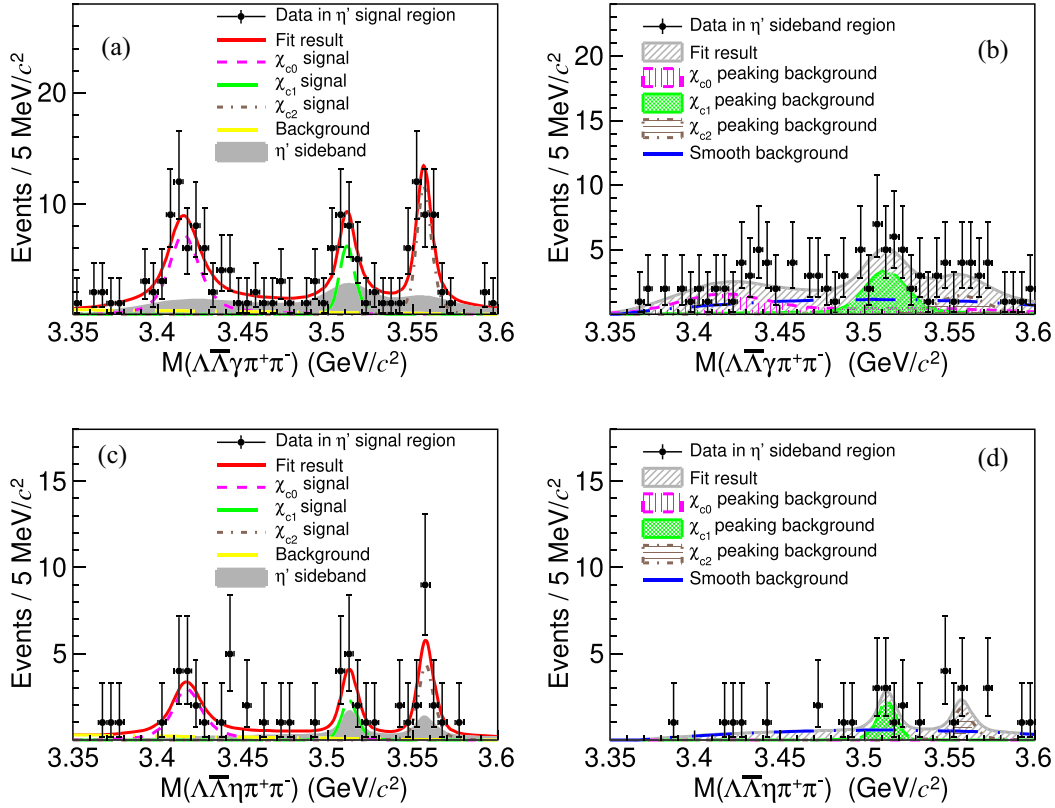


FIG. 3. Simultaneous fit to the $M(\Lambda\bar{\Lambda}\gamma\pi^+\pi^-)$ (top) and $M(\Lambda\bar{\Lambda}\eta\pi^+\pi^-)$ (bottom) distributions of the accepted candidate events in the η' (left) signal and (right) sideband regions. The dots with error bars are the data; the gray shaded histograms constitute the total contribution from the η' sideband; and the pink, green, and brown shaded histograms are the peaking background from χ_{c0} , χ_{c1} , and χ_{c2} , respectively. The solid red lines are the fit results, and the pink, green, and brown dashed lines represent the χ_{c0} , χ_{c1} , and χ_{c2} signal shapes, respectively.

region and sideband regions, respectively. Peaking backgrounds in the η' sideband regions are modeled by three $\chi_{cJ} \rightarrow \Lambda\bar{\Lambda}\gamma\pi^+\pi^-$ PHSP MC shapes plus a second-order Chebyshev polynomial, as shown in Fig. 3(b). In the η' signal region, the χ_{cJ} signal shapes are described by the corresponding MC shapes, and the smooth background is modeled by a first-order Chebyshev polynomial. The non- η' background is modeled with the same parametrized shapes in the η' sidebands, as presented in the gray shaded histograms in Figs. 3(a) and 3(b). The normalization factor between the η' signal and sideband regions is determined from a fit to the $M(\gamma\pi^+\pi^-)$ distribution in Fig. 2 (I), where the MC shape is used to describe the signal shape, and a second-order Chebyshev polynomial function is used to model the background shape. The MC shape refers to the signal distribution obtained from the MC simulation of the signal channel, corresponding to a Breit-Wigner function convolved with the detector resolution. For the PHSP MC shape, it is obtained from the MC simulation with PHSP model. The normalization factor is the ratio of background yields between the η' signal and sideband regions. An identical procedure is applied to mode II, as shown in

Figs. 3(c) and 3(d), using $M(\Lambda\bar{\Lambda}\eta\pi^+\pi^-)$ as the observable and the sideband normalization determined from the $M(\eta\pi^+\pi^-)$ distribution in Fig. 2 (II).

The number of signal events for each decay mode is expressed by

$$N_X^{\text{sig}} = N^{\text{tot}} \cdot \mathcal{B}(\psi(3686) \rightarrow \gamma\chi_{cJ}) \cdot \mathcal{B}(\chi_{cJ} \rightarrow \Lambda\bar{\Lambda}\eta') \cdot \mathcal{B}(\Lambda \rightarrow p\pi^-) \cdot \mathcal{B}(\bar{\Lambda} \rightarrow \bar{p}\pi^+) \cdot \mathcal{B}(\eta' \rightarrow X) \cdot \epsilon_X, \quad (1)$$

where X denotes the η' decay mode ($\gamma\pi^+\pi^-$ or $\eta\pi^+\pi^-$ with $\eta \rightarrow \gamma\gamma$) and ϵ_X is the corresponding detection efficiency from a mixed MC sample described below. The branching fractions of the intermediate decays are taken from the PDG [19]. The fit projections for both decay modes are shown in Fig. 3. The statistical significances of the $\chi_{cJ} \rightarrow \Lambda\bar{\Lambda}\eta'$ signals are 7.8σ , 3.5σ , and 7.6σ for $J = 0, 1$, and 2 , respectively, determined from the change in log-likelihood and the number of degrees of freedom with and without the signal component. The statistical significance does not include systematic uncertainty. The numerical fit results are listed in Table I.

TABLE I. Measured branching fractions for $\chi_{cJ} \rightarrow \Lambda \bar{\Lambda} \eta'$, where the first uncertainties are statistical, the second are systematic, S is the significance, and $R_{X(2264)}$ denotes the ratio of the $X(2264)$ -intermediate to nonresonant contribution.

Decay mode	$\mathcal{B}(\times 10^{-5})$	$R_{X(2264)}$ (%)	Efficiency (I) (%)	Efficiency (II) (%)	S(σ)	S include systematic (σ)
$\chi_{c0} \rightarrow \Lambda \bar{\Lambda} \eta'$	$7.56 \pm 1.42 \pm 0.90$	41.3	1.68	1.16	7.8	6.7
$\chi_{c1} \rightarrow \Lambda \bar{\Lambda} \eta'$	$1.54 \pm 0.51 \pm 0.16$	9.2	3.14	2.13	3.5	3.3
$\chi_{c2} \rightarrow \Lambda \bar{\Lambda} \eta'$	$3.03 \pm 0.61 \pm 0.29$	4.8	3.04	2.12	7.6	6.4

To evaluate the signal efficiency, a mixed MC sample is generated accounting for possible intermediate states. In particular, a near-threshold enhancement in the $\Lambda \bar{\Lambda}$ invariant-mass spectrum observed in $e^+e^- \rightarrow \phi \Lambda \bar{\Lambda}$ [3] is considered. To evaluate its contribution, we perform a three-dimensional (3D) unbinned maximum-likelihood fit to the distributions of $M(\Lambda \bar{\Lambda})$, $M(\Lambda \eta')$, and $M(\bar{\Lambda} \eta')$.

The mass and width of the $\Lambda \bar{\Lambda}$ enhancement are fixed at 2264 MeV/ c^2 and 73 MeV, respectively [3]. We denote this state as $X(2264)$ in the following study. The background is modeled using events from the η' sidebands with fixed shape and normalization. The signal is described as the sum of the $X(2264)$ -intermediate state and the nonresonant process, each represented by its respective PHSP

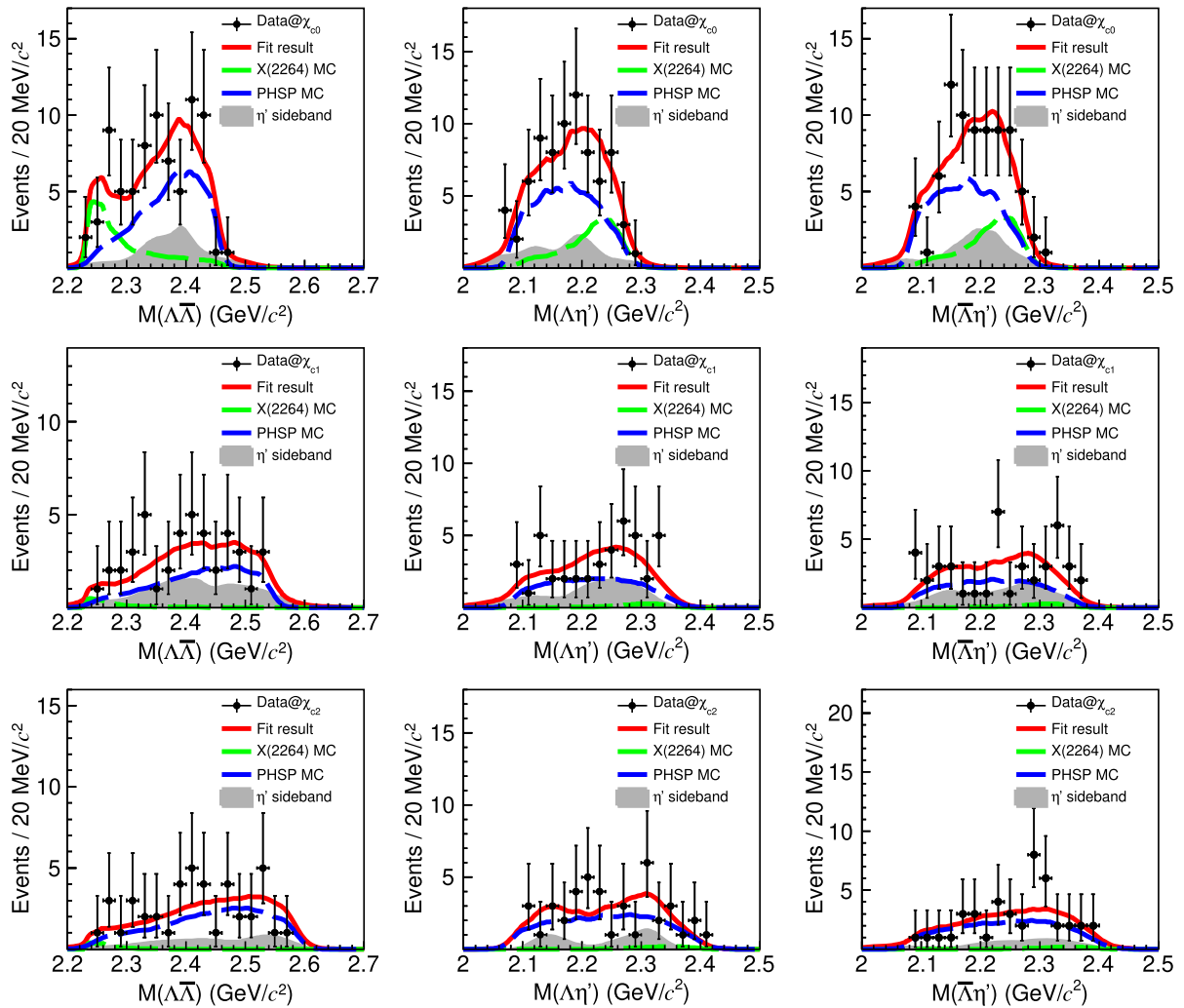


FIG. 4. The projections on two-body invariant mass of the 3D fit for each χ_{cJ} decay in the corresponding signal region. The dots with error bars are the data by combining two η' decay modes, the red solid lines are the fit results, the gray shaded histograms denote the contributions from the η' sideband, and the green and blue dashed lines represent the $X(2264)$ -intermediate state process and nonresonant process, respectively. Events have been required to be within individual χ_{cJ} signal regions.

MC shapes. The PSHP MC shapes of $X(2264)$ -intermediate and nonresonant are obtained from the MC simulation of $\chi_{cJ} \rightarrow X(2264)\eta'(X(2264) \rightarrow \Lambda\bar{\Lambda})$ and $\chi_{cJ} \rightarrow \Lambda\bar{\Lambda}\eta'$ with PHSP model, respectively. And they are modeled by the RooFit ROONDKKEYSPDF [26]. Because of limited statistics in each η' decay mode, the data from both modes are combined. The region of $[3.390, 3.445]$ GeV/ c^2 is used for χ_{c0} , $[3.495, 3.525]$ GeV/ c^2 for χ_{c1} , and $[3.540, 3.570]$ GeV/ c^2 is used for χ_{c2} . Figure 4 shows the results from the 3D fit. From the best-fit parameters, the ratio $R_{X(2264)}$ of the $X(2264)$ -intermediate to nonresonant contribution is extracted and used to mix the corresponding MC samples. The efficiencies obtained from the mixed samples and the $X(2264)$ fractions are listed in Table I.

V. SYSTEMATIC UNCERTAINTY

The systematic uncertainties in the measurements of branching fractions are listed in Table II. These uncertainties are categorized into correlated and uncorrelated sources between the two η' decay modes. The systematic uncertainties from the tracking for π^\pm , the photon detection, the Λ reconstruction, the $\bar{\Lambda}$ reconstruction, the kinematic fit, and the signal MC model are the correlated items in each η' decay mode. The combined correlated uncertainty for the two decay channels is calculated by

$$\delta_{\text{corr}} = \frac{\sum_{i=1}^2 (\delta_i \times \mathcal{B}_i \times \epsilon_i)}{\sum_{i=1}^2 (\mathcal{B}_i \times \epsilon_i)}, \quad (2)$$

where δ_i , \mathcal{B}_i , and ϵ_i represent the systematic uncertainty, branching fraction, and detection efficiency for the channel i , respectively. The systematic uncertainties from the η' mass window, the wrong photon combination,

the background veto, and the branching fraction of $\eta' \rightarrow X$ are uncorrelated items. The average of the two decay channels is calculated as

$$\delta_{\text{uncorr}} = \frac{\sqrt{\sum_{i=1}^2 (\delta_i \times \mathcal{B}_i \times \epsilon_i)^2}}{\sum_{i=1}^2 (\mathcal{B}_i \times \epsilon_i)}. \quad (3)$$

The uncertainty arising from the pion tracking is 1.0% per track with the sample of $\psi(3686) \rightarrow \pi^+\pi^-J/\psi, J/\psi \rightarrow \ell^+\ell^- (\ell = e, \mu)$ [27], for pions from η' decays. The uncertainty of photon detection is 0.5% per photon as determined by the $e^+e^- \rightarrow \gamma\mu^+\mu^-$ process [28].

The combined efficiency, including tracking for proton/antiproton and charged pion and reconstruction for Λ and $\bar{\Lambda}$, is studied by the control sample of $J/\psi \rightarrow pK^-\bar{\Lambda} + c.c.$ [29]. The relative efficiency discrepancy between data and MC simulation in each momentum and $|\cos\theta|$ bin is defined as $\Delta\epsilon_i = \frac{\epsilon_i^{\text{data}}}{\epsilon_i^{\text{MC}}} - 1$. To quantify the systematic uncertainties, we apply a normalized weighting factor $w_i = \frac{\epsilon_i}{\epsilon_{\text{tot}}}$, where ϵ_i is the MC efficiency in the i th bin and ϵ_{tot} is the total MC efficiency from our signal MC sample. The differences between data and MC simulation are subsequently evaluated by $\Sigma(w_i \times \Delta\epsilon_i)$, which are assigned as the corresponding systematic uncertainties.

To evaluate the systematic uncertainty associated with the η' mass window, we perform an unbinned maximum likelihood fit to $M(\gamma\pi^+\pi^-)$ (mode I) and $M(\eta\pi^+\pi^-)$ (mode II) distributions in data. The signal shape of η' is modeled by an MC simulated shape convolved with a Gaussian function with fitted parameters. The smooth background is parametrized by a second-order Chebychev function. Using the best-fit signal shape parameters, we generate a toy MC sample to simulate the η' line shape. The systematic

TABLE II. Relative systematic uncertainties (%) on the branching-fraction measurements. The dash (-) indicates that the source is not relevant for that decay.

Source	χ_{c0}		χ_{c1}		χ_{c2}	
	Mode I	Mode II	Mode I	Mode II	Mode I	Mode II
Tracking for π^\pm	2.0	2.0	2.0	2.0	2.0	2.0
Photon detection	1.0	1.5	1.0	1.5	1.0	1.5
Λ reconstruction	3.8	3.8	3.4	3.4	3.2	3.3
$\bar{\Lambda}$ reconstruction	0.9	0.9	0.4	0.4	0.2	0.2
η' mass window	0.6	1.0	0.6	1.0	0.6	1.0
Kinematic fit	5.2	5.3	5.0	4.2	4.8	4.7
Wrong photon	4.0	-	3.4	-	1.4	-
Background veto	1.1	0.1	1.1	0.1	1.2	0.1
Signal MC model	6.1	5.4	7.7	6.2	3.8	2.5
$\mathcal{B}(\eta' \rightarrow X)$	1.4	1.3	1.4	1.3	1.4	1.3
$\mathcal{B}(\psi(3686) \rightarrow \gamma\chi_{cJ}, \Lambda \rightarrow p\pi^-, \bar{\Lambda} \rightarrow \bar{p}\pi^+)$	2.8		3.2		2.9	
Fit procedure	6.3		8.5		5.7	
Total number of $\psi(3686)$ events	0.5		0.5		0.5	
Sum	11.9		10.6		9.7	

uncertainty is the difference in efficiency between the nominal and toy samples.

The uncertainty associated with the kinematic fit is estimated by correcting the helix parameters of charged tracks according to the method described in Ref. [30]. The difference of the detection efficiencies obtained from MC samples with and without this correction is assigned as the uncertainty.

The systematic effect of possible photon mispairing is investigated with MC truth matching. Events in which the angle between the generated and reconstructed photon $\theta_{\text{match}} < 7^\circ$ are considered correctly matched; otherwise, they are counted as mismatched. The fractions of mismatched events are 4.0%, 3.4%, and 1.4% for χ_{c0} , χ_{c1} , and χ_{c2} , respectively. These fractions are assigned as systematic uncertainties.

The background veto criteria include $M(\Lambda(\bar{\Lambda})\gamma) > 1.2 \text{ GeV}/c^2$, $|RM(\pi^+\pi^-) - m_{J/\psi}| > 10 \text{ MeV}/c^2$, $|RM(\gamma_1\gamma_2) - m_{J/\psi}| > 26 \text{ MeV}/c^2$, and $|M(\gamma_1\gamma_2) - m_{\pi^0}| > 14 \text{ MeV}/c^2$. The uncertainty from the requirement of $M(\Lambda(\bar{\Lambda})\gamma) > 1.2 \text{ GeV}/c^2$ is estimated by the control sample of $\psi(3686) \rightarrow \pi^+\pi^-J/\psi, J/\psi \rightarrow \Sigma^0\bar{\Sigma}^0$. The difference of the acceptance efficiencies between data and MC simulation is 0.01% for Σ^0 , and 0.1% for $\bar{\Sigma}^0$, which are taken as the uncertainties. Similarly, the systematic uncertainty due to the criterion $|RM(\pi^+\pi^-) - m_{J/\psi}| > 10 \text{ MeV}/c^2$ is estimated by the control sample of $\psi(3686) \rightarrow \pi^+\pi^-J/\psi, J/\psi \rightarrow \Lambda\bar{\Lambda}\eta$, the systematic uncertainty due to the criterion $|RM(\gamma_1\gamma_2) - m_{J/\psi}| > 26 \text{ MeV}/c^2$ is estimated by the control sample of $\psi(3686) \rightarrow \eta J/\psi, \eta \rightarrow \gamma\gamma, J/\psi \rightarrow \Lambda\bar{\Lambda}\pi^+\pi^-$, and the difference of the acceptance efficiencies between data and MC simulation is 0.2% for each control sample, which is taken as the corresponding uncertainty. For the selection criterion $|M(\gamma_1\gamma_2) - m_{\pi^0}| > 14 \text{ MeV}/c^2$, the difference in photon energy resolution between the data and the MC simulation can shift the $M(\gamma_1\gamma_2)$ distribution. To quantify the associated uncertainty, we enlarge the photon energy uncertainty in the reconstructed error matrix by 4% [31].

The uncertainties of the fit parameters from the 3D fit will introduce a systematic uncertainty to the efficiency. This is estimated by generating 1000 parameter sets following a multivariate Gaussian distribution with the covariance matrix from the 3D fit. Then, we propagate these variations into the efficiency calculation. The variance of the resulting efficiency distribution is adopted as the systematic uncertainty from the signal MC model.

Systematic uncertainties from branching fractions are taken from the PDG [19].

For the uncertainty of the signal shape, we modify the signal shape from the MC simulated shape to $(\text{BW} \cdot E_\gamma^3 \cdot f_d(E_\gamma)) \otimes \text{Double Gaussian}$, where BW is a Breit-Wigner function, with its parameters are fixed at the values of χ_{cJ} from PDG [19], E_γ represents the energy of the

transition photon, and $f_d(E_\gamma)$ is the damping factor [32]. The double-Gaussian function models the detector resolution, whose parameters are derived from the corresponding MC simulation. The uncertainty from the background shape is evaluated by replacing the first-order Chebyshev polynomial with a second-order one. The systematic uncertainty from the η' sideband regions is shifted by $\pm 2 \text{ MeV}/c^2$, and the maximum difference of final results is taken as the systematic uncertainty. The normalization factors between the η' signal and sideband regions are determined from the fits to the $M(\gamma\pi^+\pi^-)$ and $M(\eta\pi^+\pi^-)$ distributions with all the parameters fixed to the best values. To consider the uncertainty from the η' sideband normalization factor, we free the value of the normalization factors, and the range of sideband scale factor is the nominal normalization factor $\pm 1\sigma$, where σ is the uncertainty of the sideband normalization factor from the fits to the $M(\gamma\pi^+\pi^-)$ and $M(\eta\pi^+\pi^-)$ distributions. For any individual systematic uncertainty related to the fit procedure, the difference in the final results is taken as the systematic uncertainty. When evaluating these systematic uncertainties, we also recalculate the statistical significance. The smallest statistical significance obtained from these calculations is taken as the resulting significance that incorporates the systematic uncertainties, as presented in Table I.

The total number of $\psi(3686)$ events in data is determined with the inclusive hadronic events to be 2.7124×10^9 with an uncertainty of 0.5% [9].

The total systematic uncertainties are obtained by adding all systematic uncertainties in quadrature, assuming they are independent.

VI. CONCLUSIONS

Using a data sample of $(2.7124 \pm 0.014) \times 10^9$ $\psi(3686)$ events collected with the BESIII detector at the BEPCII collider, we have studied the decays $\chi_{cJ} \rightarrow \Lambda\bar{\Lambda}\eta'$ for $J = 0, 1, 2$ via the radiative transition $\psi(3686) \rightarrow \gamma\chi_{cJ}$. The decays $\chi_{c0,2} \rightarrow \Lambda\bar{\Lambda}\eta'$ are observed for the first time, and evidence for $\chi_{c1} \rightarrow \Lambda\bar{\Lambda}\eta'$ is found. The measured branching fractions and significances are summarized in Table I; they are significantly smaller than those for $\chi_{cJ} \rightarrow \Lambda\bar{\Lambda}\eta$ [5], $\chi_{cJ} \rightarrow \Lambda\bar{\Lambda}\omega$ [6], and $\chi_{cJ} \rightarrow \Sigma^+\bar{\Sigma}^-\eta$ [8], which have larger PHSP space. No excited baryon states nor $\Lambda\bar{\Lambda}$ near-threshold enhancement is observed within the current statistical precision, consistent with previous measurements of $\chi_{cJ} \rightarrow B\bar{B}M$ [5–8]. Further experimental studies of additional χ_{cJ} decay channels are essential to elucidate the properties of χ_{cJ} mesons, $B\bar{B}$ threshold enhancements, and possible excited baryon states.

ACKNOWLEDGMENTS

The BESIII Collaboration thanks the staff of BEPCII [33] and the IHEP computing center for their strong

support. This work is supported in part by National Key R&D Program of China under Contracts No. 2023YFA1606000 and No. 2023YFA1606704; National Natural Science Foundation of China (NSFC) under Contracts No. 12375070, No. 11635010, No. 11935015, No. 11935016, No. 11935018, No. 12025502, No. 12035009, No. 12035013, No. 12061131003, No. 12192260, No. 12192261, No. 12192262, No. 12192263, No. 12192264, No. 12192265, No. 12221005, No. 12225509, No. 12235017, and No. 12361141819; the Chinese Academy of Sciences (CAS) Large-Scale Scientific Facility Program; the Strategic Priority Research Program of Chinese Academy of Sciences under Contract No. XDA0480600; CAS under Contract No. YSBR-101; 100 Talents Program of CAS; Shanghai Leading Talent Program of Eastern Talent Plan under Contract No. JLH5913002; The Institute of Nuclear and Particle Physics (INPAC) and Shanghai Key Laboratory for Particle Physics and Cosmology; ERC under Contract No. 758462; German Research Foundation DFG under

Contract No. FOR5327; Istituto Nazionale di Fisica Nucleare, Italy; Knut and Alice Wallenberg Foundation under Contracts No. 2021.0174 and No. 2021.0299; Ministry of Development of Turkey under Contract No. DPT2006K-120470; National Research Foundation of Korea under Contract No. NRF-2022R1A2C1092335; National Science and Technology fund of Mongolia; Polish National Science Centre under Contract No. 2024/53/B/ST2/00975; STFC (United Kingdom); Swedish Research Council under Contract No. 2019.04595; and U.S. Department of Energy under Contract No. DE-FG02-05ER41374.

DATA AVAILABILITY

The data that support the findings of this article are not publicly available upon publication because it is not technically feasible and/or the cost of preparing, depositing, and hosting the data would be prohibitive within the terms of this research project. The data are available from the authors upon reasonable request.

-
- [1] M. Ablikim *et al.* (BESIII Collaboration), *Phys. Rev. Lett.* **129**, 122001 (2022).
- [2] M. Ablikim *et al.* (BESIII Collaboration), *Phys. Rev. D* **106**, 112011 (2022).
- [3] M. Ablikim *et al.* (BESIII Collaboration), *Phys. Rev. D* **104**, 152006 (2021).
- [4] M. Ablikim *et al.* (BESIII Collaboration), *Phys. Rev. D* **107**, 112011 (2023).
- [5] M. Ablikim *et al.* (BESIII Collaboration), *Phys. Rev. D* **106**, 072004 (2022).
- [6] M. Ablikim *et al.* (BESIII Collaboration), *Phys. Rev. D* **110**, 032022 (2024).
- [7] M. Ablikim *et al.* (BESIII Collaboration), *Phys. Rev. D* **110**, 032016 (2022).
- [8] M. Ablikim *et al.* (BESIII Collaboration), *Phys. Rev. D* **110**, 112013 (2024).
- [9] M. Ablikim *et al.* (BESIII Collaboration), *Chin. Phys. C* **42**, 023001 (2013); **48**, 093001 (2024).
- [10] M. Ablikim *et al.* (BESIII Collaboration), *Nucl. Instrum. Methods Phys. Res., Sect. A* **614**, 345 (2010).
- [11] C. H. Yu *et al.*, *Proceedings of IPAC2016, Busan, Korea* (2016), 10.18429/JACoW-IPAC2016-TUYA01.
- [12] M. Ablikim *et al.* (BESIII Collaboration), *Chin. Phys. C* **44**, 040001 (2020).
- [13] J. Lu, Y. Xiao, and X. Ji, *Radiat. Detect. Technol. Methods* **4**, 337 (2020).
- [14] J. W. Zhang, L. H. Wu, S. S. Sun *et al.*, *Radiat. Detect. Technol. Methods* **6**, 289 (2022).
- [15] X. Li *et al.*, *Radiat. Detect. Technol. Methods* **1**, 13 (2017). Y. X. Guo *et al.*, *Radiat. Detect. Technol. Methods* **1**, 15 (2017).
- [16] S. Agostinelli *et al.* (GEANT4 Collaboration), *Nucl. Instrum. Methods Phys. Res., Sect. A* **506**, 250 (2003).
- [17] S. Jadach, B. F. L. Ward, and Z. Was, *Phys. Rev. D* **63**, 113009 (2001); *Comput. Phys. Commun.* **130**, 260 (2000).
- [18] D. J. Lange, *Nucl. Instrum. Methods Phys. Res., Sect. A* **462**, 152 (2001); R. G. Ping, *Chin. Phys. C* **32**, 599 (2008).
- [19] S. Navas *et al.* (Particle Data Group), *Phys. Rev. D* **110**, 030001 (2024).
- [20] J. C. Chen, G. S. Huang, X. R. Qi, D. H. Zhang, and Y. S. Zhu, *Phys. Rev. D* **62**, 034003 (2000). R. L. Yang, R. G. Ping, and H. Chen, *Chin. Phys. Lett.* **31**, 061301 (2014).
- [21] E. Richter-Was, *Phys. Lett. B* **303**, 163 (1993).
- [22] W. Tanenbaum *et al.*, *Phys. Rev. D* **17**, 1731 (1978); G. R. Liao, R. G. Ping, and Y. X. Yang, *Chin. Phys. C* **26**, 051101 (2009).
- [23] M. Ablikim *et al.* (BESIII Collaboration), *Phys. Rev. Lett.* **120**, 024003 (2018).
- [24] M. Ablikim *et al.* (BESIII Collaboration), *Phys. Rev. D* **97**, 012003 (2018).
- [25] M. Xu *et al.*, *Chin. Phys. C* **33**, 428 (2009).
- [26] W. Verkerke and D. P. Kirkby, eConf **C0303241**, MOLT007 (2003).
- [27] M. Ablikim *et al.* (BESIII Collaboration), *Phys. Rev. Lett.* **105**, 261801 (2010).
- [28] M. Ablikim *et al.* (BESIII Collaboration), *J. High Energy Phys.* **08** (2024) 180.
- [29] M. Ablikim *et al.* (BESIII Collaboration), *Phys. Rev. D* **108**, 112012 (2023).

- [30] M. Ablikim *et al.* (BESIII Collaboration), *Phys. Rev. D* **87**, 012002 (2013).
 [31] M. Ablikim *et al.* (BESIII Collaboration), *Phys. Rev. Lett.* **104**, 132002 (2010).
 [32] V. V. Anashin *et al.*, *Int. J. Mod. Phys. Conf. Ser.* **02**, 188 (2011). <https://cstr.cn/31109.02.BEPC>
 [33] <https://cstr.cn/31109.02.BEPC>.

M. Ablikim,¹ M. N. Achasov,^{4,c} P. Adlarson,⁷⁹ X. C. Ai,⁸⁴ R. Aliberti,³⁷ A. Amoroso,^{78a,78c} Q. An,^{61,75,a} Y. Bai,⁶⁰ O. Bakina,³⁸ Y. Ban,^{48,h} H.-R. Bao,⁶⁷ V. Batozskaya,^{1,46} K. Begzsuren,³⁴ N. Berger,³⁷ M. Berlowski,⁴⁶ M. B. Bertani,^{30a} D. Bettoni,^{31a} F. Bianchi,^{78a,78c} E. Bianco,^{78a,78c} A. Bortone,^{78a,78c} I. Boyko,³⁸ R. A. Briere,⁵ A. Brueggemann,⁷² H. Cai,⁸⁰ M. H. Cai,^{40,k,l} X. Cai,^{1,61} A. Calcaterra,^{30a} G. F. Cao,^{1,67} N. Cao,^{1,67} S. A. Cetin,^{65a} X. Y. Chai,^{48,h} J. F. Chang,^{1,61} T. T. Chang,⁴⁵ G. R. Che,⁴⁵ Y. Z. Che,^{1,61,67} C. H. Chen,⁹ Chao Chen,⁵⁸ G. Chen,¹ H. S. Chen,^{1,67} H. Y. Chen,²¹ M. L. Chen,^{1,61,67} S. J. Chen,⁴⁴ S. M. Chen,⁶⁴ T. Chen,^{1,67} X. R. Chen,^{33,67} X. T. Chen,^{1,67} X. Y. Chen,^{12,g} Y. B. Chen,^{1,61} Y. Q. Chen,¹⁶ Z. K. Chen,⁶² J. C. Cheng,⁴⁷ L. N. Cheng,⁴⁵ S. K. Choi,¹⁰ X. Chu,^{12,g} G. Cibinetto,^{31a} F. Cossio,^{78c} J. Cottee-Meldrum,⁶⁶ H. L. Dai,^{1,61} J. P. Dai,⁸² X. C. Dai,⁶⁴ A. Dbeysi,¹⁹ R. E. de Boer,³ D. Dedovich,³⁸ C. Q. Deng,⁷⁶ Z. Y. Deng,¹ A. Denig,³⁷ I. Denisenko,³⁸ M. Destefanis,^{78a,78c} F. De Mori,^{78a,78c} X. X. Ding,^{48,h} Y. Ding,⁴² Y. X. Ding,³² J. Dong,^{1,61} L. Y. Dong,^{1,67} M. Y. Dong,^{1,61,67} X. Dong,⁸⁰ M. C. Du,¹ S. X. Du,⁸⁴ S. X. Du,^{12,g} X. L. Du,⁸⁴ Y. Y. Duan,⁵⁸ Z. H. Duan,⁴⁴ P. Egorov,^{38,b} G. F. Fan,⁴⁴ J. J. Fan,²⁰ Y. H. Fan,⁴⁷ J. Fang,^{1,61} J. Fang,⁶² S. S. Fang,^{1,67} W. X. Fang,¹ Y. Q. Fang,^{1,61} L. Fava,^{78b,78c} F. Feldbauer,³ G. Felici,^{30a} C. Q. Feng,^{61,75} J. H. Feng,¹⁶ L. Feng,^{40,k,l} Q. X. Feng,^{40,k,l} Y. T. Feng,^{61,75} M. Fritsch,³ C. D. Fu,¹ J. L. Fu,⁶⁷ Y. W. Fu,^{1,67} H. Gao,⁶⁷ Y. Gao,^{61,75} Y. N. Gao,^{48,h} Y. N. Gao,²⁰ Y. Y. Gao,³² Z. Gao,⁴⁵ S. Garbolino,^{78c} I. Garzia,^{31a,31b} L. Ge,⁶⁰ P. T. Ge,²⁰ Z. W. Ge,⁴⁴ C. Geng,⁶² E. M. Gersabeck,⁷¹ A. Gilman,⁷³ K. Goetzen,¹³ J. D. Gong,³⁶ L. Gong,⁴² W. X. Gong,^{1,61} W. Gradl,³⁷ S. Gramigna,^{31a,31b} M. Greco,^{78a,78c} M. D. Gu,⁵³ M. H. Gu,^{1,61} C. Y. Guan,^{1,67} A. Q. Guo,³³ J. N. Guo,^{12,g} L. B. Guo,⁴³ M. J. Guo,⁵² R. P. Guo,⁵¹ X. Guo,⁵² Y. P. Guo,^{12,g} A. Guskov,^{38,b} J. Gutierrez,²⁹ T. T. Han,¹ F. Hanisch,³ K. D. Hao,^{61,75} X. Q. Hao,²⁰ F. A. Harris,⁶⁹ C. Z. He,^{48,h} K. L. He,^{1,67} F. H. Heinsius,³ C. H. Heinz,³⁷ Y. K. Heng,^{1,61,67} C. Herold,⁶³ P. C. Hong,³⁶ G. Y. Hou,^{1,67} X. T. Hou,^{1,67} Y. R. Hou,⁶⁷ Z. L. Hou,¹ H. M. Hu,^{1,67} J. F. Hu,^{59,j} Q. P. Hu,^{61,75} S. L. Hu,^{12,g} T. Hu,^{1,61,67} Y. Hu,¹ Z. M. Hu,⁶² G. S. Huang,^{61,75} K. X. Huang,⁶² L. Q. Huang,^{33,67} P. Huang,⁴⁴ X. T. Huang,⁵² Y. P. Huang,¹ Y. S. Huang,⁶² T. Hussain,⁷⁷ N. Hüsken,³⁷ N. in der Wiesche,⁷² J. Jackson,²⁹ Q. Ji,¹ Q. P. Ji,²⁰ W. Ji,^{1,67} X. B. Ji,^{1,67} X. L. Ji,^{1,61} X. Q. Jia,⁵² Z. K. Jia,^{61,75} D. Jiang,^{1,67} H. B. Jiang,⁸⁰ P. C. Jiang,^{48,h} S. J. Jiang,⁹ X. S. Jiang,^{1,61,67} Y. Jiang,⁶⁷ J. B. Jiao,⁵² J. K. Jiao,³⁶ Z. Jiao,²⁵ S. Jin,⁴⁴ Y. Jin,⁷⁰ M. Q. Jing,^{1,67} X. M. Jing,⁶⁷ T. Johansson,⁷⁹ S. Kabana,³⁵ N. Kalantar-Nayestanaki,⁶⁸ X. L. Kang,⁹ X. S. Kang,⁴² M. Kavatsyuk,⁶⁸ B. C. Ke,⁸⁴ V. Khachatryan,²⁹ A. Khoukaz,⁷² O. B. Kolcu,^{65a} B. Kopf,³ M. Kuessner,³ X. Kui,^{1,67} N. Kumar,²⁸ A. Kupsc,^{46,79} W. Kühn,³⁹ Q. Lan,⁷⁶ W. N. Lan,²⁰ T. T. Lei,^{61,75} M. Lellmann,³⁷ T. Lenz,³⁷ C. Li,⁴⁹ C. Li,⁴⁵ C. H. Li,⁴³ C. K. Li,²¹ D. M. Li,⁸⁴ F. Li,^{1,61} G. Li,¹ H. B. Li,^{1,67} H. J. Li,²⁰ H. L. Li,⁸⁴ H. N. Li,^{59,j} Hui Li,⁴⁵ J. R. Li,⁶⁴ J. S. Li,⁶² J. W. Li,⁵² K. Li,¹ K. L. Li,^{40,k,l} L. J. Li,^{1,67} Lei Li,⁵⁰ M. H. Li,⁴⁵ M. R. Li,^{1,67} P. L. Li,⁶⁷ P. R. Li,^{40,k,l} Q. M. Li,^{1,67} Q. X. Li,⁵² R. Li,^{18,33} S. X. Li,¹² Shanshan Li,^{27,i} T. Li,⁵² T. Y. Li,⁴⁵ W. D. Li,^{1,67} W. G. Li,^{1,a} X. Li,^{1,67} X. H. Li,^{61,75} X. K. Li,^{48,h} X. L. Li,⁵² X. Y. Li,^{1,8} X. Z. Li,⁶² Y. Li,²⁰ Y. G. Li,^{48,h} Y. P. Li,³⁶ Z. H. Li,⁴⁰ Z. J. Li,⁶² Z. X. Li,⁴⁵ Z. Y. Li,⁸² C. Liang,⁴⁴ H. Liang,^{61,75} Y. F. Liang,⁵⁷ Y. T. Liang,^{33,67} G. R. Liao,¹⁴ L. B. Liao,⁶² M. H. Liao,⁶² Y. P. Liao,^{1,67} J. Libby,²⁸ A. Limphirat,⁶³ D. X. Lin,^{33,67} L. Q. Lin,⁴¹ T. Lin,¹ B. J. Liu,¹ B. X. Liu,⁸⁰ C. X. Liu,¹ F. Liu,¹ F. H. Liu,⁵⁶ Feng Liu,⁶ G. M. Liu,^{59,j} H. Liu,^{40,k,l} H. B. Liu,¹⁵ H. H. Liu,¹ H. M. Liu,^{1,67} Huihui Liu,²² J. B. Liu,^{61,75} J. J. Liu,²¹ K. Liu,^{40,k,l} K. Liu,⁷⁶ K. Y. Liu,⁴² Ke Liu,²³ L. Liu,⁴⁰ L. C. Liu,⁴⁵ Lu Liu,⁴⁵ M. H. Liu,³⁶ P. L. Liu,¹ Q. Liu,⁶⁷ S. B. Liu,^{61,75} W. M. Liu,^{61,75} W. T. Liu,⁴¹ X. Liu,^{40,k,l} X. K. Liu,^{40,k,l} X. L. Liu,^{12,g} X. Y. Liu,⁸⁰ Y. Liu,^{40,k,l} Y. Liu,⁸⁴ Y. B. Liu,⁴⁵ Z. A. Liu,^{1,61,67} Z. D. Liu,⁹ Z. Q. Liu,⁵² Z. Y. Liu,⁴⁰ X. C. Lou,^{1,61,67} H. J. Lu,²⁵ J. G. Lu,^{1,61} X. L. Lu,¹⁶ Y. Lu,⁷ Y. H. Lu,^{1,67} Y. P. Lu,^{1,61} Z. H. Lu,^{1,67} C. L. Luo,⁴³ J. R. Luo,⁶² J. S. Luo,^{1,67} M. X. Luo,⁸³ T. Luo,^{12,g} X. L. Luo,^{1,61} Z. Y. Lv,²³ X. R. Lyu,^{67,p} Y. F. Lyu,⁴⁵ Y. H. Lyu,⁸⁴ F. C. Ma,⁴² H. L. Ma,¹ Heng Ma,^{27,i} J. L. Ma,^{1,67} L. L. Ma,⁵² L. R. Ma,⁷⁰ Q. M. Ma,¹ R. Q. Ma,^{1,67} R. Y. Ma,²⁰ T. Ma,^{61,75} X. T. Ma,^{1,67} X. Y. Ma,^{1,61} Y. M. Ma,³³ F. E. Maas,¹⁹ I. MacKay,⁷³ M. Maggiora,^{78a,78c} S. Malde,⁷³ Q. A. Malik,⁷⁷ H. X. Mao,^{40,k,l} Y. J. Mao,^{48,h} Z. P. Mao,¹ S. Marcello,^{78a,78c} A. Marshall,⁶⁶ F. M. Melendi,^{31a,31b} Y. H. Meng,⁶⁷ Z. X. Meng,⁷⁰ G. Mezzadri,^{31a} H. Miao,^{1,67} T. J. Min,⁴⁴ R. E. Mitchell,²⁹ X. H. Mo,^{1,61,67} B. Moses,²⁹ N. Yu. Muchnoi,^{4,c} J. Muskalla,³⁷ Y. Nefedov,³⁸ F. Nerling,^{19,e} Z. Ning,^{1,61} S. Nisar,^{11,m} Q. L. Niu,^{40,k,l} W. D. Niu,^{12,g} Y. Niu,⁵² C. Normand,⁶⁶ S. L. Olsen,^{10,67} Q. Ouyang,^{1,61,67} S. Pacetti,^{30b,30c} X. Pan,⁵⁸ Y. Pan,⁶⁰ A. Pathak,¹⁰ Y. P. Pei,^{61,75} M. Pelizaeus,³ H. P. Peng,^{61,75} X. J. Peng,^{40,k,l}

Y. Y. Peng,^{40,k,l} K. Peters,^{13,e} K. Petridis,⁶⁶ J. L. Ping,⁴³ R. G. Ping,^{1,67} S. Plura,³⁷ V. Prasad,³⁶ F. Z. Qi,¹ H. R. Qi,⁶⁴ M. Qi,⁴⁴ S. Qian,^{1,61} W. B. Qian,⁶⁷ C. F. Qiao,⁶⁷ J. H. Qiao,²⁰ J. J. Qin,⁷⁶ J. L. Qin,⁵⁸ L. Q. Qin,¹⁴ L. Y. Qin,^{61,75} P. B. Qin,⁷⁶ X. P. Qin,⁴¹ X. S. Qin,⁵² Z. H. Qin,^{1,61} J. F. Qiu,¹ Z. H. Qu,⁷⁶ J. Rademacker,⁶⁶ C. F. Redmer,³⁷ A. Rivetti,^{78c} M. Rolo,^{78c} G. Rong,^{1,67} S. S. Rong,^{1,67} F. Rosini,^{30b,30c} Ch. Rosner,¹⁹ M. Q. Ruan,^{1,61} N. Salone,^{46,q} A. Sarantsev,^{38,d} Y. Schelhaas,³⁷ K. Schoenning,⁷⁹ M. Scodreggio,^{31a} W. Shan,²⁶ X. Y. Shan,^{61,75} Z. J. Shang,^{40,k,l} J. F. Shangguan,¹⁷ L. G. Shao,^{1,67} M. Shao,^{61,75} C. P. Shen,^{12,g} H. F. Shen,^{1,8} W. H. Shen,⁶⁷ X. Y. Shen,^{1,67} B. A. Shi,⁶⁷ H. Shi,^{61,75} J. L. Shi,^{12,g} J. Y. Shi,¹ S. Y. Shi,⁷⁶ X. Shi,^{1,61} H. L. Song,^{61,75} J. J. Song,²⁰ M. H. Song,⁴⁰ T. Z. Song,⁶² W. M. Song,³⁶ Y. X. Song,^{48,h,n} Zirong Song,^{27,i} S. Sosio,^{78a,78c} S. Spataro,^{78a,78c} S. Stansilauš,⁷³ F. Stielor,³⁷ S. S. Su,⁴² G. B. Sun,⁸⁰ G. X. Sun,¹ H. Sun,⁶⁷ H. K. Sun,¹ J. F. Sun,²⁰ K. Sun,⁶⁴ L. Sun,⁸⁰ R. Sun,⁷⁵ S. S. Sun,^{1,67} T. Sun,^{54,f} W. Y. Sun,⁵³ Y. C. Sun,⁸⁰ Y. H. Sun,³² Y. J. Sun,^{61,75} Y. Z. Sun,¹ Z. Q. Sun,^{1,67} Z. T. Sun,⁵² C. J. Tang,⁵⁷ G. Y. Tang,¹ J. Tang,⁶² J. J. Tang,^{61,75} L. F. Tang,⁴¹ Y. A. Tang,⁸⁰ L. Y. Tao,⁷⁶ M. Tat,⁷³ J. X. Teng,^{61,75} J. Y. Tian,^{61,75} W. H. Tian,⁶² Y. Tian,³³ Z. F. Tian,⁸⁰ I. Uman,^{65b} B. Wang,¹ B. Wang,⁶² Bo Wang,^{61,75} C. Wang,^{40,k,l} C. Wang,²⁰ Cong Wang,²³ D. Y. Wang,^{48,h} H. J. Wang,^{40,k,l} J. Wang,⁹ J. J. Wang,⁸⁰ J. K. Wang,^{12,g} J. P. Wang,⁵² K. Wang,^{1,61} L. L. Wang,¹ L. W. Wang,³⁶ M. Wang,⁵² M. Wang,^{61,75} N. Y. Wang,⁶⁷ S. Wang,^{12,g} S. Wang,^{40,k,l} T. Wang,^{12,g} T. J. Wang,⁴⁵ J. K. Wang,^{12,g} W. Wang,⁶² W. P. Wang,³⁷ X. Wang,^{48,h} X. F. Wang,^{40,k,l} X. L. Wang,^{12,g} X. N. Wang,^{1,67} Xin Wang,^{27,i} Y. Wang,¹ Y. D. Wang,⁴⁷ Y. F. Wang,^{1,8,67} Y. H. Wang,^{40,k,l} Y. J. Wang,^{61,75} Y. L. Wang,²⁰ Y. N. Wang,⁴⁷ Y. N. Wang,⁸⁰ Yaqian Wang,¹⁸ Yi Wang,⁶⁴ Yuan Wang,^{18,33} Z. Wang,^{1,61} Z. Wang,⁴⁵ Z. L. Wang,² Z. Q. Wang,^{12,g} Z. Y. Wang,^{1,67} Ziyi Wang,⁶⁷ D. Wei,⁴⁵ D. H. Wei,¹⁴ H. R. Wei,⁴⁵ F. Weidner,⁷² S. P. Wen,¹ U. Wiedner,³ G. Wilkinson,⁷³ M. Wolke,⁷⁹ J. F. Wu,^{1,8} L. H. Wu,¹ L. J. Wu,^{1,67} L. J. Wu,²⁰ Lianjie Wu,²⁰ S. G. Wu,^{1,67} S. M. Wu,⁶⁷ X. Wu,^{12,g} Y. J. Wu,³³ Z. Wu,^{1,61} L. Xia,^{61,75} B. H. Xiang,^{1,67} D. Xiao,^{40,k,l} G. Y. Xiao,⁴⁴ H. Xiao,⁷⁶ Y. L. Xiao,^{12,g} Z. J. Xiao,⁴³ C. Xie,⁴⁴ K. J. Xie,^{1,67} Y. Xie,⁵² Y. G. Xie,^{1,61} Y. H. Xie,⁶ Z. P. Xie,^{61,75} T. Y. Xing,^{1,67} C. J. Xu,⁶² G. F. Xu,¹ H. Y. Xu,² M. Xu,^{61,75} Q. J. Xu,¹⁷ Q. N. Xu,³² T. D. Xu,⁷⁶ X. P. Xu,⁵⁸ Y. Xu,^{12,g} Y. C. Xu,⁸¹ Z. S. Xu,⁶⁷ F. Yan,²⁴ L. Yan,^{12,g} W. B. Yan,^{61,75} W. C. Yan,⁸⁴ W. H. Yan,⁶ W. P. Yan,²⁰ X. Q. Yan,^{1,67} H. J. Yang,^{54,f} H. L. Yang,³⁶ H. X. Yang,¹ J. H. Yang,⁴⁴ R. J. Yang,²⁰ Y. Yang,^{12,g} Y. H. Yang,⁴⁴ Y. Q. Yang,⁹ Y. Z. Yang,²⁰ Z. P. Yao,⁵² M. Ye,^{1,61} M. H. Ye,^{8,a} Z. J. Ye,^{59,j} Junhao Yin,⁴⁵ Z. Y. You,⁶² B. X. Yu,^{1,61,67} C. X. Yu,⁴⁵ G. Yu,¹³ J. S. Yu,^{27,i} L. W. Yu,^{12,g} T. Yu,⁷⁶ X. D. Yu,^{48,h} Y. C. Yu,⁸⁴ Y. C. Yu,⁴⁰ C. Z. Yuan,^{1,67} H. Yuan,^{1,67} J. Yuan,³⁶ J. Yuan,⁴⁷ L. Yuan,² M. K. Yuan,^{12,g} S. H. Yuan,⁷⁶ Y. Yuan,^{1,67} C. X. Yue,⁴¹ Ying Yue,²⁰ A. A. Zafar,⁷⁷ F. R. Zeng,⁵² S. H. Zeng,⁶⁶ X. Zeng,^{12,g} Yujie Zeng,⁶² Y. J. Zeng,^{1,67} Y. C. Zhai,⁵² Y. H. Zhan,⁶² Shunan Zhang,⁷³ B. L. Zhang,^{1,67} B. X. Zhang,^{1,a} D. H. Zhang,⁴⁵ G. Y. Zhang,²⁰ G. Y. Zhang,^{1,67} H. Zhang,^{61,75} H. Zhang,⁸⁴ H. C. Zhang,^{1,61,67} H. H. Zhang,⁶² H. Q. Zhang,^{1,61,67} H. R. Zhang,^{61,75} H. Y. Zhang,^{1,61} J. Zhang,⁶² J. J. Zhang,⁵⁵ J. L. Zhang,²¹ J. Q. Zhang,⁴³ J. S. Zhang,^{12,g} J. W. Zhang,^{1,61,67} J. X. Zhang,^{40,k,l} J. Y. Zhang,¹ J. Z. Zhang,^{1,67} Jianyu Zhang,⁶⁷ L. M. Zhang,⁶⁴ Lei Zhang,⁴⁴ N. Zhang,⁸⁴ P. Zhang,^{1,8} Q. Zhang,²⁰ Q. Y. Zhang,³⁶ R. Y. Zhang,^{40,k,l} S. H. Zhang,^{1,67} Shulei Zhang,^{27,i} X. M. Zhang,¹ X. Y. Zhang,⁵² Y. Zhang,¹ Y. Zhang,⁷⁶ Y. T. Zhang,⁸⁴ Y. H. Zhang,^{1,61} Y. P. Zhang,^{61,75} Z. D. Zhang,¹ Z. H. Zhang,¹ Z. L. Zhang,³⁶ Z. L. Zhang,⁵⁸ Z. X. Zhang,²⁰ Z. Y. Zhang,⁸⁰ Z. Y. Zhang,⁴⁵ Z. Z. Zhang,⁴⁷ Zh. Zh. Zhang,²⁰ G. Zhao,¹ J. Y. Zhao,^{1,67} J. Z. Zhao,^{1,61} L. Zhao,¹ L. Zhao,^{61,75} M. G. Zhao,⁴⁵ S. J. Zhao,⁸⁴ Y. B. Zhao,^{1,61} Y. L. Zhao,⁵⁸ Y. X. Zhao,^{33,67} Z. G. Zhao,^{61,75} A. Zhemchugov,^{38,b} B. Zheng,⁷⁶ B. M. Zheng,³⁶ J. P. Zheng,^{1,61} W. J. Zheng,^{1,67} X. R. Zheng,²⁰ Y. H. Zheng,^{67,p} B. Zhong,⁴³ C. Zhong,²⁰ H. Zhou,^{37,52,o} J. Q. Zhou,³⁶ S. Zhou,⁶ X. Zhou,⁸⁰ X. K. Zhou,⁶ X. R. Zhou,^{61,75} X. Y. Zhou,⁴¹ Y. X. Zhou,⁸¹ Y. Z. Zhou,^{12,g} A. N. Zhu,⁶⁷ J. Zhu,⁴⁵ K. Zhu,¹ K. J. Zhu,^{1,61,67} K. S. Zhu,^{12,g} L. Zhu,³⁶ L. X. Zhu,⁶⁷ S. H. Zhu,⁷⁴ T. J. Zhu,^{12,g} W. D. Zhu,^{12,g} W. J. Zhu,¹ W. Z. Zhu,²⁰ Y. C. Zhu,^{61,75} Z. A. Zhu,^{1,67} X. Y. Zhuang,⁴⁵ J. H. Zou,¹ and J. Zu^{61,75}

(BESIII Collaboration)

¹*Institute of High Energy Physics, Beijing 100049, People's Republic of China*²*Beihang University, Beijing 100191, People's Republic of China*³*Bochum Ruhr-University, D-44780 Bochum, Germany*⁴*Budker Institute of Nuclear Physics SB RAS (BINP), Novosibirsk 630090, Russia*⁵*Carnegie Mellon University, Pittsburgh, Pennsylvania 15213, USA*⁶*Central China Normal University, Wuhan 430079, People's Republic of China*⁷*Central South University, Changsha 410083, People's Republic of China*⁸*China Center of Advanced Science and Technology, Beijing 100190, People's Republic of China*⁹*China University of Geosciences, Wuhan 430074, People's Republic of China*¹⁰*Chung-Ang University, Seoul, 06974, Republic of Korea*

- ¹¹COMSATS University Islamabad,
Lahore Campus, Defence Road, Off Raiwind Road, 54000 Lahore, Pakistan
- ¹²Fudan University, Shanghai 200433, People's Republic of China
- ¹³GSI Helmholtzcentre for Heavy Ion Research GmbH, D-64291 Darmstadt, Germany
- ¹⁴Guangxi Normal University, Guilin 541004, People's Republic of China
- ¹⁵Guangxi University, Nanning 530004, People's Republic of China
- ¹⁶Guangxi University of Science and Technology, Liuzhou 545006, People's Republic of China
- ¹⁷Hangzhou Normal University, Hangzhou 310036, People's Republic of China
- ¹⁸Hebei University, Baoding 071002, People's Republic of China
- ¹⁹Helmholtz Institute Mainz, Staudinger Weg 18, D-55099 Mainz, Germany
- ²⁰Henan Normal University, Xinxiang 453007, People's Republic of China
- ²¹Henan University, Kaifeng 475004, People's Republic of China
- ²²Henan University of Science and Technology, Luoyang 471003, People's Republic of China
- ²³Henan University of Technology, Zhengzhou 450001, People's Republic of China
- ²⁴Hengyang Normal University, Hengyang 421001, People's Republic of China
- ²⁵Huangshan College, Huangshan 245000, People's Republic of China
- ²⁶Hunan Normal University, Changsha 410081, People's Republic of China
- ²⁷Hunan University, Changsha 410082, People's Republic of China
- ²⁸Indian Institute of Technology Madras, Chennai 600036, India
- ²⁹Indiana University, Bloomington, Indiana 47405, USA
- ^{30a}INFN Laboratori Nazionali di Frascati, I-00044, Frascati, Italy
- ^{30b}INFN Sezione di Perugia, I-06100, Perugia, Italy
- ^{30c}University of Perugia, I-06100, Perugia, Italy
- ^{31a}INFN Sezione di Ferrara, I-44122, Ferrara, Italy
- ^{31b}University of Ferrara, I-44122, Ferrara, Italy
- ³²Inner Mongolia University, Hohhot 010021, People's Republic of China
- ³³Institute of Modern Physics, Lanzhou 730000, People's Republic of China
- ³⁴Institute of Physics and Technology, Mongolian Academy of Sciences,
Peace Avenue 54B, Ulaanbaatar 13330, Mongolia
- ³⁵Instituto de Alta Investigación, Universidad de Tarapacá, Casilla 7D, Arica 1000000, Chile
- ³⁶Jilin University, Changchun 130012, People's Republic of China
- ³⁷Johannes Gutenberg University of Mainz, Johann-Joachim-Becher-Weg 45, D-55099 Mainz, Germany
- ³⁸Joint Institute for Nuclear Research, 141980 Dubna, Moscow region, Russia
- ³⁹Justus-Liebig-Universitaet Giessen,
II. Physikalisches Institut, Heinrich-Buff-Ring 16, D-35392 Giessen, Germany
- ⁴⁰Lanzhou University, Lanzhou 730000, People's Republic of China
- ⁴¹Liaoning Normal University, Dalian 116029, People's Republic of China
- ⁴²Liaoning University, Shenyang 110036, People's Republic of China
- ⁴³Nanjing Normal University, Nanjing 210023, People's Republic of China
- ⁴⁴Nanjing University, Nanjing 210093, People's Republic of China
- ⁴⁵Nankai University, Tianjin 300071, People's Republic of China
- ⁴⁶National Centre for Nuclear Research, Warsaw 02-093, Poland
- ⁴⁷North China Electric Power University, Beijing 102206, People's Republic of China
- ⁴⁸Peking University, Beijing 100871, People's Republic of China
- ⁴⁹Qufu Normal University, Qufu 273165, People's Republic of China
- ⁵⁰Renmin University of China, Beijing 100872, People's Republic of China
- ⁵¹Shandong Normal University, Jinan 250014, People's Republic of China
- ⁵²Shandong University, Jinan 250100, People's Republic of China
- ⁵³Shandong University of Technology, Zibo 255000, People's Republic of China
- ⁵⁴Shanghai Jiao Tong University, Shanghai 200240, People's Republic of China
- ⁵⁵Shanxi Normal University, Linfen 041004, People's Republic of China
- ⁵⁶Shanxi University, Taiyuan 030006, People's Republic of China
- ⁵⁷Sichuan University, Chengdu 610064, People's Republic of China
- ⁵⁸Soochow University, Suzhou 215006, People's Republic of China
- ⁵⁹South China Normal University, Guangzhou 510006, People's Republic of China
- ⁶⁰Southeast University, Nanjing 211100, People's Republic of China
- ⁶¹State Key Laboratory of Particle Detection and Electronics,
Beijing 100049, Hefei 230026, People's Republic of China
- ⁶²Sun Yat-Sen University, Guangzhou 510275, People's Republic of China
- ⁶³Suranaree University of Technology, University Avenue 111, Nakhon Ratchasima 30000, Thailand

- ⁶⁴*Tsinghua University, Beijing 100084, People's Republic of China*
- ^{65a}*Turkish Accelerator Center Particle Factory Group, Istinye University, 34010, Istanbul, Turkey*
- ^{65b}*Near East University, Nicosia, North Cyprus, 99138, Mersin 10, Turkey*
- ⁶⁶*University of Bristol, H H Wills Physics Laboratory, Tyndall Avenue, Bristol, BS8 1TL, UK*
- ⁶⁷*University of Chinese Academy of Sciences, Beijing 100049, People's Republic of China*
- ⁶⁸*University of Groningen, NL-9747 AA Groningen, The Netherlands*
- ⁶⁹*University of Hawaii, Honolulu, Hawaii 96822, USA*
- ⁷⁰*University of Jinan, Jinan 250022, People's Republic of China*
- ⁷¹*University of Manchester, Oxford Road, Manchester, M13 9PL, United Kingdom*
- ⁷²*University of Muenster, Wilhelm-Klemm-Strasse 9, 48149 Muenster, Germany*
- ⁷³*University of Oxford, Keble Road, Oxford OX13RH, United Kingdom*
- ⁷⁴*University of Science and Technology Liaoning, Anshan 114051, People's Republic of China*
- ⁷⁵*University of Science and Technology of China, Hefei 230026, People's Republic of China*
- ⁷⁶*University of South China, Hengyang 421001, People's Republic of China*
- ⁷⁷*University of the Punjab, Lahore-54590, Pakistan*
- ^{78a}*University of Turin and INFN, University of Turin, I-10125, Turin, Italy*
- ^{78b}*University of Eastern Piedmont, I-15121, Alessandria, Italy*
- ^{78c}*INFN, I-10125, Turin, Italy*
- ⁷⁹*Uppsala University, Box 516, SE-75120 Uppsala, Sweden*
- ⁸⁰*Wuhan University, Wuhan 430072, People's Republic of China*
- ⁸¹*Yantai University, Yantai 264005, People's Republic of China*
- ⁸²*Yunnan University, Kunming 650500, People's Republic of China*
- ⁸³*Zhejiang University, Hangzhou 310027, People's Republic of China*
- ⁸⁴*Zhengzhou University, Zhengzhou 450001, People's Republic of China*

^aDeceased.

^bAlso at the Moscow Institute of Physics and Technology, Moscow 141700, Russia.

^cAlso at the Novosibirsk State University, Novosibirsk, 630090, Russia.

^dAlso at the NRC "Kurchatov Institute", PNPI, 188300, Gatchina, Russia.

^eAlso at Goethe University Frankfurt, 60323 Frankfurt am Main, Germany.

^fAlso at Key Laboratory for Particle Physics, Astrophysics and Cosmology, Ministry of Education; Shanghai Key Laboratory for Particle Physics and Cosmology; Institute of Nuclear and Particle Physics, Shanghai 200240, People's Republic of China.

^gAlso at Key Laboratory of Nuclear Physics and Ion-beam Application (MOE) and Institute of Modern Physics, Fudan University, Shanghai 200443, People's Republic of China.

^hAlso at State Key Laboratory of Nuclear Physics and Technology, Peking University, Beijing 100871, People's Republic of China.

ⁱAlso at School of Physics and Electronics, Hunan University, Changsha 410082, China.

^jAlso at Guangdong Provincial Key Laboratory of Nuclear Science, Institute of Quantum Matter, South China Normal University, Guangzhou 510006, China.

^kAlso at MOE Frontiers Science Center for Rare Isotopes, Lanzhou University, Lanzhou 730000, People's Republic of China.

^lAlso at Lanzhou Center for Theoretical Physics, Lanzhou University, Lanzhou 730000, People's Republic of China.

^mAlso at the Department of Mathematical Sciences, IBA, Karachi 75270, Pakistan.

ⁿAlso at Ecole Polytechnique Federale de Lausanne (EPFL), CH-1015 Lausanne, Switzerland.

^oAlso at Helmholtz Institute Mainz, Staudinger Weg 18, D-55099 Mainz, Germany.

^pAlso at Hangzhou Institute for Advanced Study, University of Chinese Academy of Sciences, Hangzhou 310024, China.

^qCurrently at Silesian University in Katowice, Chorzow, 41-500, Poland.